Accepted Manuscript

Ab initio study of interstitial cluster interaction with Re, Os, and Ta in W

W. Setyawan, G. Nandipati, R.J. Kurtz

PII: S0022-3115(16)31044-3

DOI: 10.1016/j.jnucmat.2016.11.002

Reference: NUMA 49989

To appear in: *Journal of Nuclear Materials*

Received Date: 14 April 2016

Revised Date: 24 October 2016

Accepted Date: 1 November 2016

Please cite this article as: W. Setyawan, G. Nandipati, R.J. Kurtz, Ab initio study of interstitial cluster interaction with Re, Os, and Ta in W, *Journal of Nuclear Materials* (2016), doi: 10.1016/j.jnucmat.2016.11.002.

Ab Initio Study of Interstitial Cluster Interaction with Re, Os, and Ta in W

W. Setyawan[1,*], G. Nandipati[1], and R. J. Kurtz[1]

[1]*Pacific Northwest National Laboratory, P. O. Box 999, Richland, WA 99352, USA*
[*]*Corresponding author, Tel.: +1(509)3717692; Fax.: +1(509)3753033; E-mail address: wahyu.setyawan@pnnl.gov*

Abstract

The stability of tungsten self-interstitial atom (SIA) clusters is studied using first-principles methods. Clusters from one to seven SIAs are systematically explored from 1264 unique configurations. Finite-size effect of the simulation cell is corrected based on the scaling of formation energy versus inverse volume cell. Furthermore, the accuracy of the calculations is improved by treating the 5p semicore states as valence states. Configurations of the three most stable clusters in each cluster size *n* are presented, which consist of parallel [111] dumbbells. The evolution of these clusters leading to small dislocation loops is discussed. The binding energy of size-*n* clusters is analyzed relative to an $n \rightarrow (n\text{-}1) + 1$ dissociation and is shown to increase with size. Extrapolation for $n > 7$ is presented using a dislocation loop model. In addition, the interaction of these clusters with a substitutional Re, Os, or Ta solute is explored by replacing one of the dumbbells with the solute. Rhenium and Os strongly attract these clusters, but Ta strongly repels. The strongest interaction is found when the solute is located on the periphery of the cluster rather than in the middle. The magnitude of this interaction decreases with cluster size. Empirical fits to describe the trend of the solute binding energy are presented.

Keywords: fusion; tungsten; interstitial cluster; structure; stability; dissociation; solute; binding energy; density functional theory; finite-size scaling; semicore states

1. Introduction

Understanding defect dynamics is fundamental in predicting the evolution of various defect structures in a material. The existence of defects can be beneficial, for instance a dopant in semiconductors, or detrimental, such as solid or gaseous transmutation products in reactor materials. In this research, we focus on the latter case, in particular for tungsten. Current fusion energy system designs utilize tungsten as a plasma-facing material [1-4]. Naturally occurring tungsten is made up of five stable isotopes: ^{180}W (0.1%), ^{182}W (26.3%), ^{183}W (14.3%), ^{184}W (30.7%), and ^{186}W (28.6%). Under fusion neutron irradiation, tungsten undergoes (n, γ) and (n, 2n) transmutation reactions that mainly produce rhenium and osmium isotopes [5, 6]. Neutron absorption in ^{180}W produces traces of Ta through β^+ decay of ^{181}W [5]. Therefore, Re, Os, and to a lesser extent Ta, are the main concerns in regards to the effects of transmutation products on tungsten properties degradation. These solutes will eventually lead to the formation of brittle intermetallic phases that is detrimental to the mechanical properties of tungsten [7, 8].

Transmutation products also influence the nature of atomic displacement damage accumulation during neutron irradiation. Experiments performed in the JOYO reactor found that accumulation

of vacancies results in the formation of a void lattice [9-11], however, this phenomenon was not observed in HFIR irradiations [7, 12, 13]. It was inferred that due to the higher thermal neutron content of the HFIR neutron spectrum, solid transmutation products were generated at a high enough rate to suppress void lattice formation. Presumably, whether or not a void lattice forms depends on a rate-dependent dynamical balance between vacancy generation and distribution (including migration and dissociation of vacancies from smaller vacancy clusters and growth of larger clusters), one-dimensional (1D) diffusion of self interstitial atoms (SIAs) that engrave the distributed vacancies into a void lattice, and other defects that alter the vacancy distribution as well as the carving efficiency of the SIAs. Therefore, predicting the evolutionary and combinatorial effects of transmutation products and intrinsic defects requires knowledge of how they interact with each other.

A great number of vacancies and interstitials are generated as a result of high-energy collisions between neutrons and tungsten atoms. Various sizes and morphologies of these defects are produced [14-17] each with its own characteristics of diffusion [12, 18-22], dissociation [20, 23], and binding [12, 23, 24]. Recently, ab initio data on the interaction of an individual vacancy or SIA with transition metal elements were reported [24]. It was found that an SIA would have to overcome at least a binding energy of approximately 0.82 and 1.65 eV to detach from a Re and Os substitutional solute, respectively. Less is known about the interaction of clusters of SIAs with these solutes. For instance, does a cluster of SIAs bind less strongly to a solute than individual SIAs do? What is the asymptotic model of the binding energy? These questions are particularly relevant for tungsten because, similar to an SIA, SIA clusters are also highly mobile [22, 25].

To our knowledge, ab initio data on the interaction of SIA clusters with solutes are absent, understandably because of the high computational cost to explore various structures of such clusters. In [23], the binding energy of an SIA within an SIA cluster was reported, however, no details were given about the configuration or how the configuration was chosen. Here, we present the results of a systematic search of the structure and stability of SIA clusters up to size seven and their binding properties to a substitutional Re, Os, or Ta solute.

2. Methods

The stability of SIA clusters is studied within the density functional theory (DFT) framework. VASP.5.4.1 [26, 27] software is used to solve the Kohn-Sham equations with plane-wave basis sets. Projector-augmented-wave (PAW) [27] pseudo-potentials for W, Re, Os, and Ta are taken from VASP's library potpaw_PBE_v5.2.12. Perdew-Burke-Ernzerhof (PBE) functionals [28] are employed for the electronic exchange-correlation energies.

2.1. Convergence study

Defect formation energies are calculated using cubic 5x5x5 supercells of tungsten's body-centered cubic (bcc) unit cell. A perfect crystal consists of 250 W atoms. The coordinates of the atoms and box volume are optimized while maintaining cubic symmetry. In our opinion, maintaining cubic symmetry is more appropriate than relaxing cell shape because the defect is

assumed to be isolated. In other simulations in which the defect concentration matters, relaxing cell shape is appropriate since high enough concentration of defect may induce a phase transformation of the whole crystal. Nevertheless, both relaxation procedures should give the same results for large enough cell or after finite size effect has been corrected for infinitely large cell. The relaxation is stopped when the norm of the force on each atom is < 0.025 eV/Å and the external pressure acting on the box is < 0.5 kbar. At the end of the relaxations, a static calculation is performed to eliminate errors due to plane-wave basis incompleteness associated with volume changes. A Monkhorst-Pack [29] **k**-point grid is employed to sample the Brillouin zone.

The energy cutoff (*ENCUT*) of the plane waves is carefully determined following a convergence study of the formation energies of [111], [110], and [100] W dumbbells. The results are presented in Table 1, along with the results from [30] in which the data were obtained using the same pseudo-potential, supercell size, and relaxation procedure as employed here. *ENCUT* = 250 eV is found to be sufficient to converge the formation energies to within 20 meV. In fact, one may use a slightly lower cutoff of 225 eV if only differences between the formation energies are of interest. We note that the maximum plane-wave energy of the pseudo-potentials for W, Ta, Re, and Os is very similar to one another, namely 223, 224, 226, and 228 eV respectively. Consequently, the energy convergence behavior of a system containing Ta, Re, and/or Os is expected to be very similar to pure W. The **k**-points are determined from a convergence of the formation energy of the [111] dumbbell. The results are shown in the bottom panel in Table 1. A 5x5x5 **k**-point grid is sufficient to converge the formation energy within 20 meV. Therefore, we set *ENCUT* = 250 eV and **k**-points = 5x5x5 for calculations with the 5x5x5 supercells. The bulk of the calculations to explore the various configurations of SIA clusters are performed using the 5x5x5 supercell (cell555). The total number of unique SIA cluster configurations explored in this study is 12,559. Through a systematic reduction that will be described in Section 3, there are 1,264 clusters that are evaluated with DFT.

Table 1. (top panel) Convergence tests of the plane-wave energy cutoff (*ENCUT*) with 5x5x5 cells and 3x3x3 **k**-points. Formation energy (E_f) of [111], [110], and [100] dumbbells, and a vacancy in tungsten. The *ENCUT* in bold converges the E_f to within 20 meV. (bottom panel) Convergence tests of **k**-points for the E_f of [111] dumbbell. The **k**-points in bold converge the E_f to within 20 meV.

E_f (eV)	*ENCUT* (eV)						
	200	225	**250**	300	350	500	450 Ref [30]
111	9.95	10.03	10.00	10.00	10.01	10.01	9.98
110 - 111	0.26	0.24	0.25	0.26	0.25	0.26	N/A
100 - 111	1.85	1.98	1.99	2.00	2.00	2.00	N/A
Vacancy	3.32	3.31	3.30	3.32	3.32	3.31	3.34
	ENCUT (eV)	**k**-points					
		3x3x3	4x4x4	**5x5x5**	6x6x6	7x7x7	
111	250	10.00	9.80	9.90	9.91	9.91	
	300	10.00	9.79	9.89	9.91	9.91	
	500	10.01	9.81	9.91	9.92	9.92	

2.2. Finite size correction

The finite size of the supercell introduces elastic interactions between periodic arrays of displacement fields. This finite size effect is particularly significant for interstitial defects with extended displacement fields [31-34]. In an elastically isotropic medium, the elastic interaction between two displacement fields is proportional to the inverse volume [35, 36]. Using this relation, the correction to the defect formation energy can be obtained by plotting the formation energy as a function of inverse volume. To obtain the finite size correction, we employ 4x4x4, 5x5x5, and 6x6x6 supercells (i.e. cell444, cell555, and cell666). The formation energy of the [111] dumbbell is used to determine the **k**-points for each supercell. The convergence is studied up to 8x8x8, 7x7x7, and 7x7x7 **k**-points for cell444, cell555, and cell666, respectively. The formation energy is converged to within 0.02 eV with **k**-points = 6x6x6 for cell444, 5x5x5 for cell555 as previously described, and 5x5x5 for cell666.

Figure 1 shows the finite size scaling for the most stable clusters of SIAs (the procedure find the most stable clusters is later described in Section 3). The plotted values are the formation energy per the number of SIAs. A linear scaling is evident from Figure 1. The formation energies, and consequently binding energies, reported in Sections 3 and 4 are calculated using the same finite size scaling approach. The error in the formation energy per SIA associated with the fitting is typically 0.01 eV or less for all cluster sizes.

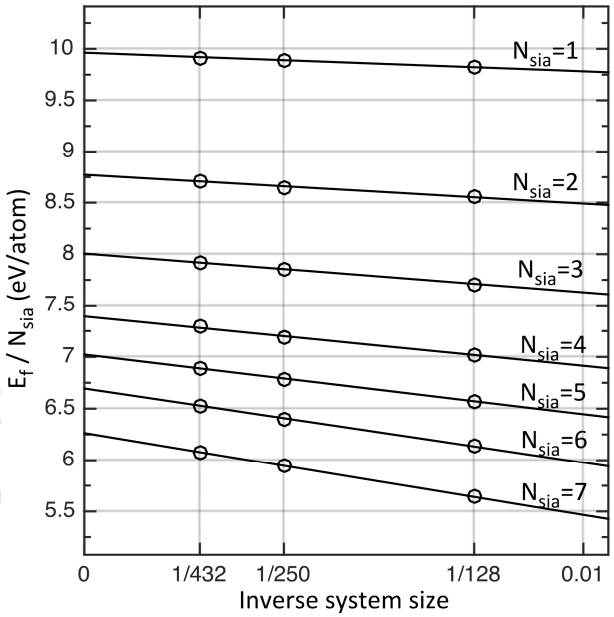

Figure 1. Formation energy of self-interstitial clusters per the number of interstitial atoms in the cluster as a function of system size (number of atoms in an undefected supercell). Fit lines show a linear scaling with respect to inverse system size.

2.3. Semicore states

The bulk of the calculations are performed using the standard version of the paw_PBE_v5.2.12 potentials, in which electrons in 6s and 5d states are treated as valence electrons. It was shown that including the 5p orbitals in the valence states is important to obtain accurate formation energies of SIAs in tungsten [24, 31, 33]. Gharaee et al reported that the effect of semicore states is only weakly dependent on the **k**-points and system size [31]. Our calculations with cell444 and cell555 support their finding. For instance, the difference in the semicore effect using those supercells is < 0.01 eV for formation energy of [111] dumbbell. The semicore effect on binding energy is 0.01 eV for size-2 SIA clusters, < 0.01 eV for Re binding to a size-1 or size-2 SIA clusters. Therefore, the effect of semicore states for all the energies presented in Sections 3 and 4, is calculated using cell444 with 6x6x6 **k**-points.

3. Results

3.1. Size-2 Clusters

To explore configurations of two SIAs, a group of 10 lattice sites as shown in Figure 2a is used to select the location of the dumbbells. This group encompasses up to the fifth nearest-neighbor distance (nn5), i.e. from atom 1 to atom 81. To begin, we pick n = 2 site combinations out of the m = 10 sites. Subsequently, non-equivalent site combinations are identified based on bond lengths. In this case, there are five unique combinations. Then, we construct dumbbells at those sites. Given that the most stable dumbbell orientation in W is [111], we focus on clusters of <111> dumbbells. Permuting the <111> orientations of the dumbbells at those sites gives a total of 4x4x5 = 80 possible clusters. Unique clusters are identified based on the list of bonds in the cluster, resulting in 23 unique clusters, which are then relaxed.

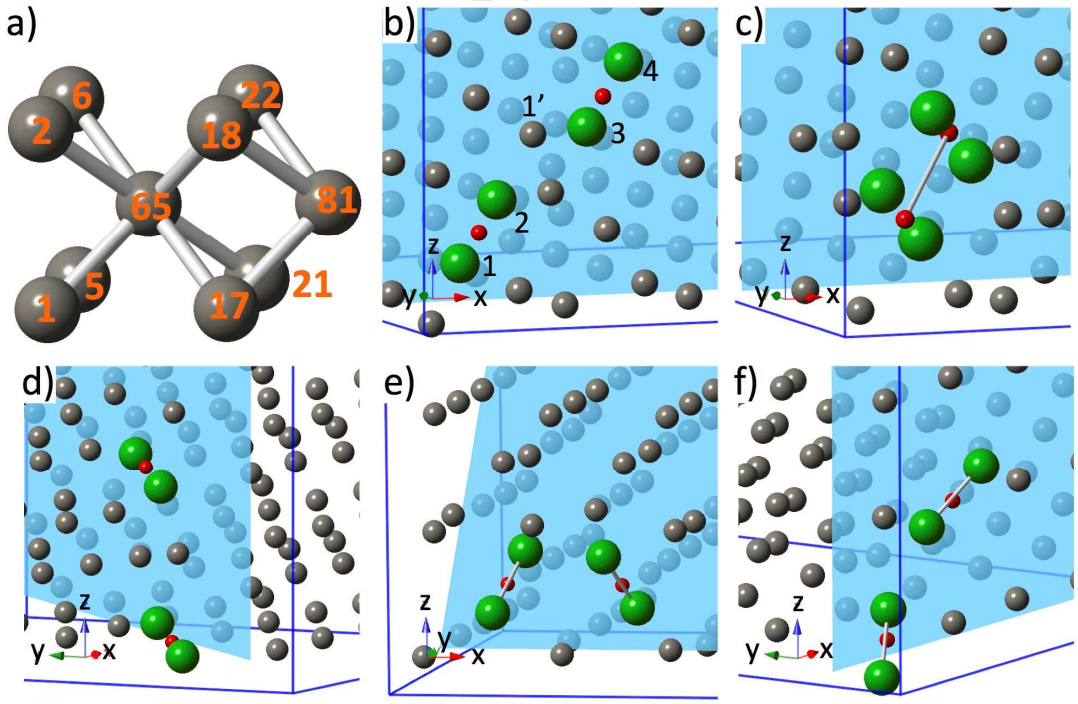

Figure 2. a) Lattice sites from which configurations of size-2 interstitial clusters are searched.

The five most stable clusters are shown in order from b) to f). The orientations are b) both [111], c) both [11-1], d) both [111], e) [111] and [11-1], and f) [111] and [1-11]. The most stable cluster is shown in b), it consists of dumbbell atoms labeled as 1, 2, 3, and 4. In b), if the 1-2 dumbbell translates one hop along [111], i.e. atom 2 forms a new dumbbell with atom 1', the resulting cluster is equivalent to the one shown in c).

The five most stable configurations are shown in Figures 2b through 2f, in which the dumbbell atoms are rendered as green spheres with the location of the dumbbell sites depicted as small red dots. The most stable size-2 cluster (MSC-2) consists of a [111] dumbbell at site 1 and another [111] dumbbell at site 18, i.e. the third nearest-neighbor distance (nn3) apart. We note that this finding is consistent with the pair correlation function of SIA defects generated in a displacement cascade [15]. In that study, the dominant peak in the pair correlation function occurs at nn3.

The stability of a size-*n* cluster is studied by calculating its binding energy with respect to an $n \rightarrow (n\text{-}1) + 1$ reaction as follows

$$E_b\{n\} = E_t\{n-1\} + E_t\{1\} - E_t\{n\} - E_t\{0\} \quad (1)$$

where $E_t\{n\}$ is the total energy of a supercell containing a size-*n* cluster and $E_t\{0\}$ is the total energy of a perfect supercell. A positive $E_b\{n\}$ denotes that a size-*n* cluster is more stable than a configuration consisting of a size-(*n*-1) cluster and a separate SIA. Note that the dissociation energy for an SIA to separate from a size-*n* cluster will be equal to $E_b\{n\} + E_m\{1\}$, where $E_m\{1\}$ is the migration energy of an SIA. For each cluster size, the binding energies of the three most stable configurations are summarized in Table 2.

Table 2. Binding energy of a size-*n* cluster conrresponding to an $n \rightarrow (n\text{-}1) + 1$ reaction. All energies are in eV. The results for the three most stable (1st, 2nd, and 3rd) configurations are presented. Results are extrapolated based on finite size scaling using 4x4x4 cell (6x6x6 **k**-points), 5x5x5 cell (5x5x5 **k**-points), and 6x6x6 cell (5x5x5 **k**-points). Calculations with and without 5p semicore states are denoted as w/sc and w/o sc, respectively. The semicore corrections were obtained using the 4x4x4 cell (6x6x6 **k**-points).

n	w/o sc			w/sc		
	1st	2nd	3rd	1st	2nd	3rd
2	2.38	2.35	1.84	2.45	2.42	1.86
3	3.49	2.87	2.33	3.65	2.94	2.46
4	4.42	4.33	3.03	4.60	4.51	3.18
5	4.41	3.50	3.17	4.60	3.67	3.33
6	4.90	4.76	4.51	5.13	5.00	4.74
7	6.29	4.78	4.67	6.52	5.02	4.90

The binding energy of the MSC-2 indicates that dissociation of this cluster into two [111] dumbbells is highly unlikely. The second most stable cluster is a pair of [11-1] dumbbells separated at the first nn distance (Figure 2c). The third most stable cluster consists of a pair of [111] dumbbells at the fourth nn distance (Figure 2d). The fourth stable cluster consists of [111] and [11-1] dumbbells at the second nn distance (Figure 2e). The fifth stable cluster consists of [111] and [1-11] dumbbells at the third nn separation (Figure 2f).

The results indicate that these clusters are strongly bound. The strongest clusters are found when the dumbbells are oriented in parallel. In fact, the three most stable clusters all form in parallel configurations. However, a collinear cluster exhibits repulsion even at a large separation distance. For instance, since the displacement field induced by a [111] dumbbell is highly directional along [111] and [-1-1-1] [24, 32, 34], we may estimate the range of repulsion of collinear dumbbells as follows. Consider a [111] dumbbell in a cell555 where this dumbbell together with its periodic images form an infinite array of collinear [111] dumbbells. In such a case, the difference in the formation energy using a cell555 and an infinitely large cell (obtained from finite-size scaling) is approximately equal to the binding energy of an infinite array of collinear [111] dumbbells, which for cell555 two collinear dumbbells are separated at the 10^{th} hop along [111] (~ 28 Å). This binding energy is -0.06 eV (without semicore states) and -0.08 eV (with semicore states). While the binding energy within such an array is not exactly the same as the binding energy between two isolated collinear dumbbells, it gives an estimate of the range of the repulsion of collinear dumbbells ~ 28 Å, or the range of influence of a single dumbbell to be half of this distance, i.e. ~ 14 Å, which is in a fairly good agreement with the estimated range reported in [24] of ~ 11 Å. Such a range of influence is larger than that in Fe (~ 7 Å [34, 37]). Hence our calculation further corroborates the comparison of the atomic displacement for the <111> string of atoms induced by a <111> dumbbell among bcc metals [32] which shows that the extent of a <111> dumbbell in the 4d and 5d metals is larger than that in the 3d metals.

To verify the assumption that clusters of [111] dumbbells form the most stable cluster, we explore clusters consisting of a [111] and a [110] dumbbells (db111db110), as well as clusters of two [110] dumbbells (db110db110). For the db111db110 case, permuting <111> and <110> orientations at the five two-site combinations, as previously described, results in 120 clusters out of which 37 clusters are unique. After relaxing these clusters, the three most stable clusters are found to be the same as the three most stable clusters shown in Figure 2c-2d. In other words, the [110] dumbbell has rotated so that it is aligned with the [111] counterpart. For the db110db110 exploration, there are 180 clusters in which 38 clusters are unique. After relaxation, the three most stable clusters are again found in the parallel [111] configurations as shown in Figure 2c-2d. These results clearly indicate that the clusters prefer configurations that consist of [111] dumbbells. Therefore, to explore size-3 clusters, only [111] dumbbells are considered.

3.2. Size-3 Clusters

As previously noted, in searching for size-2 clusters, site 81 is included so that we can explore a pair of dumbbells up to the fifth nearest neighbor, which is the distance between site 1 to site 81. The results of size-2 clusters show that the five most stable configurations do not involve any pair separated at the fifth nearest neighbor. Therefore, site 81 is excluded in exploring size-3 clusters. In other words, candidates for size-3 clusters are identified from nine lattice sites forming a body-centered cube, as shown in Figure 2a but without site 81. Taking combinations of three out of nine sites gives 84 combinations which reduces to six unique cases, namely (1, 65, 17), (1, 65, 18), (1, 65, 22), (1, 17, 18), (1, 17, 22), and (1, 18, 6). Permuting the <111> orientations of the dumbbells at those sites results in 384 clusters, which reduce to 101 unique configurations, which are then relaxed. Note that the results from the size-2 clusters suggest that

clusters prefer parallel configurations. To verify this finding, here in exploring size-3 clusters, all non-parallel orientations are included.

The most stable size-3 cluster (MSC-3) is shown in Figure 3a. The configuration consists of [11-1] dumbbells forming an isosceles triangle on a (01-1) plane. The lengths of the triangle's sides correspond to nn1, nn1, and nn2. The second and third most stable clusters are shown in Figures 3b and 3c, respectively. The cluster in Figure 3b consists of [111] dumbbells forming an isosceles triangle on a (110) plane with side lengths corresponding to nn1, nn1, and nn3. One may construct an equivalent cluster to this one by arranging [11-1] dumbbells on a (01-1) plane. Therefore, this cluster has the same dumbbell orientation and arrangement plane as MSC-3 but differs in the location of the dumbbells. The cluster in Figure 3c forms a linear configuration of [11-1] dumbbells along [111]. Comparing these clusters, we observe that a more compact configuration provides increased stability.

All clusters in Figure 3 may be seen to belong to a family of clusters consisting of [11-1] dumbbells arranged on a (01-1) plane. In this family, the dumbbells are oriented approximately 35^{o} off normal (i.e. from the plane's normal). A different family of clusters can be derived from [11-1] dumbbells arranged on a (11-1) plane, i.e. the dumbbells are parallel to the plane's normal, also known as prismatic clusters. For a size-3 prismatic cluster, the most compact configuration consists of [11-1] dumbbells forming an equilateral triangle with side length equaling nn3 (e.g. occupying sites 5, 17, and 22 in Figure 2a). The binding energy of such a cluster is E_b = -0.29 eV (without semicore states) and -0.21 eV (with semicore states). Note that even though these values of binding energy suggest that this cluster is unstable with respect to MSC-1 and MSC2, it is still highly binding with respect to three separate [111] dumbbells (i.e. E_b = 2.09 eV (without semicore) and 2.17 eV (with semicore)). The results from size-3 clusters support the finding from size-2 clusters in that parallel configurations of <111> dumbbells are much more stable than non-parallel configurations. Therefore, to explore size-4 and larger clusters, we focus on parallel dumbbells.

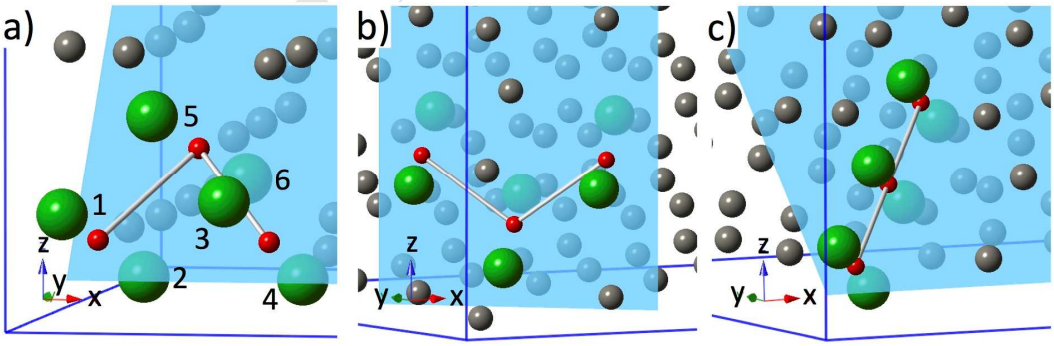

Figure 3. Three most stable configuration of size-3 self-interstitial clusters. The bonds are drawn between dumbbells that are located within the first nearest-neighbor distance. In a), the dumbbell atoms are labeled from 1 to 6 and will be used when discussing the binding property of this cluster with a substitutional Re, Os, or Ta.

3.3. Larger Clusters

Size-4 clusters are explored from two sets of lattice site. In the first set, the locations for the dumbbells are searched from 12 lattice sites shown in Figure 4a. The 12 sites are located on a (01-1) plane. This is motivated from the results of size-3 clusters in which the three most stable clusters form [11-1] dumbbells on the (01-1) plane. Hence, in this set we focus on [11-1] dumbbells. Combination of 4 out of 12 sites gives 495 combinations out of which 90 are unique. In the second set, the locations of the dumbbells are explored from 16 lattice sites forming a 2x2x2 cubic supercell (Figure 4b). Combination of 4 out of 16 is 1820, which reduces to 83 unique combinations. Unlike in the first set, the orientation of the dumbbells is not limited to [11-1]. In the second set, parallel configurations of [111], [11-1], [1-11], and [-111] dumbbells are allowed. Hence there are 4x83 = 332 parallel clusters in which 254 are unique. The three most stable configurations obtained from the first set are shown in Figure 5a to 5c. From the second set, we also found the same configurations as shown in Figure 5a to 5c as the three most stable clusters.

For this reason, candidates for larger clusters are generated from a collection of [11-1] dumbbells on a (01-1) plane, similar to the first set of size-4 clusters. For size-5, size-6, and size-7 clusters, there are 792, 924, and 792 site combinations, respectively. Clusters are constructed by placing [11-1] dumbbells at those sites. Even after eliminating equivalent clusters, the number of unique clusters in each group remains large. There are 181, 259, and 269 unique clusters, respectively.

Figure 5 shows three of the most stable clusters for each size; panels a) to c), d) to f), g) to i), and j) to l) for size-4, size-5, size-6, and size-7, respectively. In Figure 5, for non-planar clusters, arrows are drawn to point to the projected location of the dumbbells onto the corresponding plane. In each row, the clusters are presented in the order of their stability, with the most stable configuration plotted in the first column (panels a), d), g), and j)). The binding energies for these clusters are summarized in Table 2. The most stable cluster for size-4, size-5, size-6, and size-7 is referred to as MSC-4, MSC-5, MSC-6, and MSC-7, respectively.

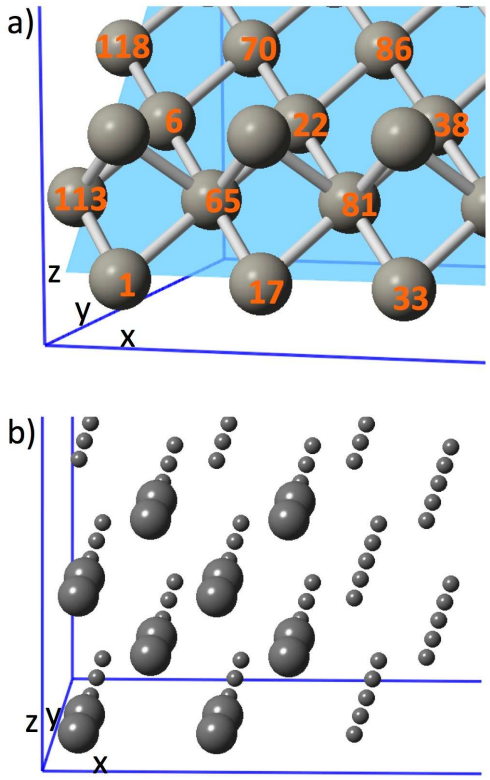

Figure 4. a) The 12 lattice sites on a (01-1) plane from which candidate configurations of size-4 to size-7 clusters are searched. b) The 16 lattice sites (rendered with larger spheres) forming a 2x2x2 cubic supercell from which additional candidate configurations of size-4 clusters are searched.

Even though we start with planar configurations, the majority of the clusters transform into non-planar configurations. More specifically, the dumbbells are arranged in two layers of {110} planes. In fact, MSC-4, MSC-5, MSC-6, and MSC-7 are all non-planar. The arrangement of MSC-7 can be seen as four [11-1] dumbbells on a (01-1) plane and three [11-1] dumbbells on an adjacent (01-1) plane. It can also be seen as [11-1] dumbbells arranged on three (11-1) planes forming a perfect prismatic cluster. Using the dumbbell numbering scheme shown for MSC-7, smaller prismatic clusters can be identified. For example, a size-3 prismatic cluster corresponds to the assemblage formed by dumbbells 1-2, 3-4, and 5-6. This cluster is previously described in section 3.2. A size-4 prismatic cluster is formed by dumbbells 7-8, 9-10, 13-14, and 11-12, constituting a perfect tetrahedron with E_b = 2.53 eV (without semicore states) and 2.66 eV (with semicore states). The binding energy of this tetrahedral cluster is much smaller than that of MSC-4. Therefore, it appears that, the results from size-4 to size-7 clusters confirm the results from size-2 and size-3 clusters in that small clusters of interstitials prefer parallel configurations of <111> dumbbells on {110} planes, with the dumbbells oriented ~35^o off normal.

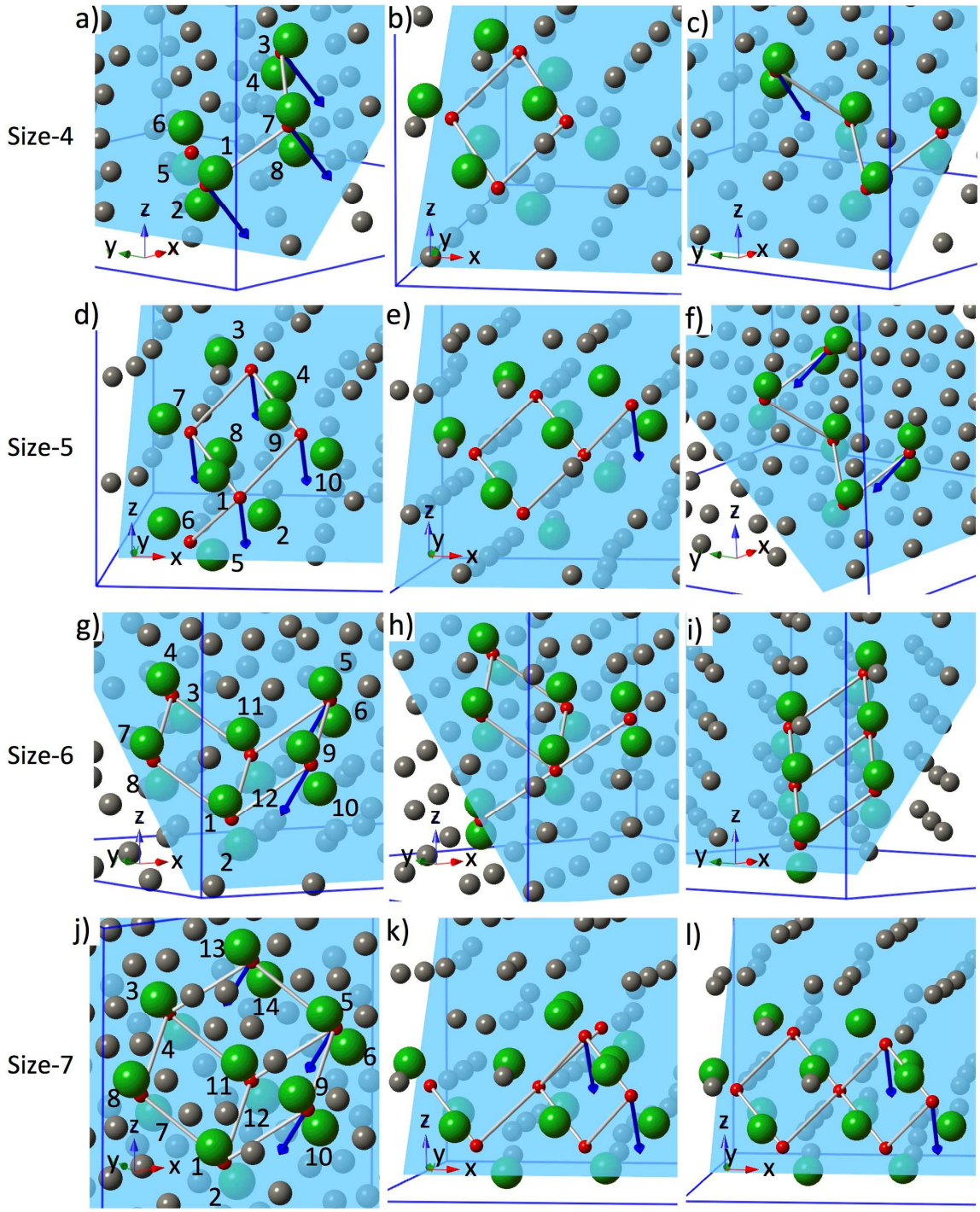

Figure 5. Three most stable configurations for SIA clusters shown in the order of decreasing stability from the first to the third column. For non-planar clusters, arrows are drawn to point to the projected location of the dumbbells on the corresponding plane. The bonds are drawn between dumbbells that are located within the first nearest-neighbor distance. The binding energies are shown in Table 2. In a), d), g), and j), the numbering scheme of the dumbbell atoms is shown and will be used in the discussion.

3.4. Interaction with Substitutional Solute Re, Os, and Ta

When an SIA binds to a substitutional solute positioned along its migration path, it forms a mixed dumbbell. Thus, in a mixed dumbbell, the solute atom adopts an interstitial position. For brevity, a mixed dumbbell of Re refers to a Re-W dumbbell. The formation energy of a mixed dumbbell is calculated from

$$E_f\{dbx\} = E_t\{dbx\} - E_{t,W} - E_{sol} \quad (2)$$

where $E_t\{dbx\}$ is the total energy of the supercell containing a mixed dumbbell, and $E_{t,W}$ is the total energy of a pure supercell, and E_{sol} is the total energy per atom of the solute in its groundstate structure, i.e. Re and Os in hexagonal close-packed structure and Ta in bcc. Similarly, the formation energy of a substitutional solute is calculated from

$$E_{f,s} = E_{t,s} - E_{t,W}\frac{N_0 - 1}{N_0} - E_{sol} \quad (3)$$

where $E_{t,s}$ is the total energy of the supercell containing a substitutional solute and N_0 is the number of W atoms in a pure supercell. Table 3 shows the $E_f\{dbx\}$ in [100], [110], and [111] orientations and $E_{f,s}$ for Ta, Re, and Os.

Table 3. Formation energies of Ta-W, W-W, Re-W, and Os-W dumbells in the [111], [110], and [100] orientations, as well as the formation energies of a substitutional Ta, Re, and Os, and a vacancy in W. All energies are in eV. Values in **bold** are the formation energies corresponding to the most stable orientation of these dumbbells. Note that the Ta-W [100] dumbbell instantaneously relaxes to a W-W [100] dumbbell and a substitutional Ta. Results are extrapolated based on the finite size scaling using 4x4x4 cell (6x6x6 **k**-points), 5x5x5 cell (5x5x5 **k**-points), and 6x6x6 cell (5x5x5 **k**-points). Calculations with and without 5p semicore states are denoted as w/sc and w/o sc, respectively. The semicore corrections were obtained using the 4x4x4 cell (6x6x6 **k**-points).

	w/o sc				w/sc			
	Ta-W	W-W	Re-W	Os-W	Ta-W	W-W	Re-W	Os-W
111	**10.12** (10.04[a])	**9.96** (9.89[a])	9.32 (9.30[a])	9.06	**10.38** (10.34[a])	**10.21** (10.16[a])	9.56 (9.53[a])	9.26
110	10.54 (10.53[a])	10.23 (10.25[a])	**9.24** (9.30[a])	**8.70**	10.93 (11.01[a])	10.51 (10.59[a])	**9.46** (9.55[a])	**8.86**
100	11.38	12.03	11.28	10.88	11.36	12.22	11.44	10.99
Substitutional	-0.47 (-0.46[a])	0.00	0.17 (0.17[a])	0.75	-0.47 (-0.47[a])	0.00	0.18 (0.17[a])	0.76
Vacancy	N/A	3.17	N/A	N/A	N/A	3.15	N/A	N/A

[a] are extrapolated results from [31] in which the finite size scaling was obtained using 3x3x3, 4x4x4, and 5x5x5 cells all with 6x6x6 **k**-points, and the semicore states corrections were obtained using 4x4x4 cell with 3x3x3 **k**-points.

The formation energy of substitutional solutes in W increases from Ta → Re → Os. While the opposite trend is observed for the [111] and [110] dumbbells where their formation energy decreases from Ta-W → W-W → Re-W → Os-W. For the [100], W-W, Re-W, and Os-W dumbbells also follow a decreasing trend, while the Ta-W does not. The anomalous behavior of

Ta-W [100] dumbbell is caused by the fact that, unlike all other dumbbells listed in Table 3 in which the solute is part of the mixed dumbbell, the Ta-W [100] dumbbell instantaneously relaxes to a W-W [100] dumbbell and a substitutional Ta. The most stable orientation for a Ta-W dumbbell is [111], while for Re-W and Os-W it is [110].

Similar to the case of an SIA, when an SIA cluster binds to a substitutional solute located along its migration path, the solute adopts an interstitial site and becomes part of the dumbbell atoms. Therefore, the binding property of SIA clusters with a substitutional solute is studied by replacing one of the conjugate atoms with Re, Os, or Ta. Conjugate atoms are those initially at lattice sites but now sharing the sites with SIAs as dumbbells. The binding energy of a size-*n* cluster with a substitutional solute is calculated from

$$E_b\{\alpha{:}\, n, sol\} = E_t\{\alpha{:}\, n\} + E_{t,s} - E_t\{\alpha{:}\, n, sol\} - E_t\{0\} \quad (4)$$

where $E_t\{\alpha{:}n\}$ is the total energy of the supercell containing a size-*n* cluster in α configuration, $E_t\{\alpha{:}n,sol\}$ is similar to $E_t\{\alpha{:}n\}$ but with one of the conjugate atoms replaced by a solute, $E_{t,s}$ is the total energy of the supercell containing a substitutional solute, and $E_t\{0\}$ is the total energy of a perfect supercell. For example in a size-3 cluster, there are six dumbbell atoms in which three are the actual interstitial atoms and the other three are the conjugate atoms, when we replace one of the dumbbell atoms with a solute, we mean to replace one of these conjugate atoms. Therefore, the size of the cluster remains three. Clearly, from this configuration, depending on the reference state selected, one may calculate a binding energy with respect to a size-2 SIA cluster and a mixed dumbbell, instead of with respect to a size-3 SIA cluster and a substitutional solute. The binding energy defined in Equation (4) refers to the latter case and is the binding energy that will be discussed in the following paragraphs. Further justification and importance of the chosen definition of binding energy will be apparent in Section 4 when we compare different definitions of binding energies.

Three of the most stable clusters for each cluster size are considered and their binding with a solute atom is explored. From these three clusters, the minimum, maximum, and average binding energies are calculated. The results are presented in the top panel of Table 4. Even within a given cluster size, solute binding varies depending on the location of the solute in the cluster. This is illustrated by the data given in the bottom panel of Table 4 in which the minimum, maximum, and average values are presented only for the MSCs.

Table 4. Binding energy of size-*n* SIA clusters to a substitutional solute obtained by replacing one of the dumbbell atoms with the solute. The minimum, maximum, and average values are in eV and calculated from the three most stable configurations (top panel) and from the most stable configuration only (bottom panel). Results are extrapolated based on the finite size scaling using 4x4x4 cell (6x6x6 **k**-points), 5x5x5 cell (5x5x5 **k**-points), and 6x6x6 cell (5x5x5 **k**-points). Calculations with and without 5p semicore states are denoted as w/sc and w/o sc, respectively. The semicore corrections were obtained using the 4x4x4 cell (6x6x6 **k**-points).

w/o sc									
n	Re			Os			Ta		
	Min	Max	Ave	Min	Max	Ave	Min	Max	Ave

1	0.81	0.81	0.81	1.65	1.65	1.65	-0.63	-0.63	-0.63
2	0.74	0.86	0.80	1.67	1.75	1.73	-0.74	-0.59	-0.64
3	0.66	0.91	0.79	1.39	1.82	1.61	-0.67	-0.52	-0.61
4	0.69	0.83	0.78	1.43	1.67	1.58	-0.66	-0.53	-0.60
5	0.55	0.80	0.74	1.16	1.64	1.51	-0.66	-0.43	-0.60
6	0.56	0.78	0.71	1.14	1.58	1.47	-0.65	-0.47	-0.59
7	0.43	0.77	0.67	0.87	1.56	1.40	-0.65	-0.41	-0.56
2	0.74	0.86	0.80	1.75	1.75	1.75	-0.66	-0.60	-0.64
3	0.81	0.83	0.82	1.68	1.69	1.69	-0.64	-0.62	-0.63
4	0.69	0.79	0.76	1.48	1.66	1.56	-0.64	-0.53	-0.59
5	0.60	0.79	0.74	1.42	1.57	1.52	-0.66	-0.56	-0.61
6	0.56	0.78	0.72	1.14	1.58	1.46	-0.65	-0.47	-0.59
7	0.43	0.74	0.67	0.87	1.50	1.41	-0.61	-0.43	-0.56
					w/sc				
1	0.83	0.83	0.83	1.71	1.71	1.71	-0.64	-0.64	-0.64
2	0.77	0.89	0.83	1.74	1.82	1.80	-0.75	-0.60	-0.65
3	0.68	0.93	0.81	1.43	1.87	1.66	-0.68	-0.52	-0.62
4	0.71	0.85	0.80	1.46	1.70	1.61	-0.66	-0.54	-0.60
5	0.57	0.82	0.76	1.20	1.68	1.55	-0.66	-0.43	-0.60
6	0.58	0.80	0.72	1.17	1.61	1.50	-0.65	-0.48	-0.60
7	0.46	0.80	0.70	0.90	1.60	1.43	-0.65	-0.41	-0.56
2	0.77	0.89	0.83	1.82	1.82	1.82	-0.70	-0.62	-0.66
3	0.83	0.85	0.84	1.73	1.73	1.73	-0.64	-0.63	-0.64
4	0.71	0.81	0.77	1.52	1.69	1.60	-0.65	-0.54	-0.59
5	0.62	0.81	0.77	1.46	1.61	1.56	-0.66	-0.56	-0.61
6	0.58	0.80	0.73	1.17	1.61	1.49	-0.65	-0.48	-0.59
7	0.46	0.77	0.69	0.90	1.54	1.44	-0.61	-0.43	-0.56

From Table 4, it is evident that Re binds strongly to SIA clusters but the strength decreases with increasing cluster size. Osmium shows a similar binding trend, but stronger than Re. On the other hand, SIA clusters are strongly repelled by Ta on their migration path with the magnitude of the repulsion decreasing for larger clusters. The interaction for Ta exhibits a comparable magnitude to that of Re, but with an opposite sign. While the interaction for Os is about twice that of Re. Comparing these interactions with the difference in the electronic valence of Ta, Re, and Os with respect to W, namely -1, +1, and +2, suggests that the binding properties of these solutes are closely related to the electronic band structures. We note that this valence difference does not necessarily reflect the difference in Pauling electronegativity. The Pauling electronegativity is 1.5 (Ta), 2.36 (W), 1.9 (Re), and 2.2 (Os). Clearly Ta, Re, and Os are all less electronegative compared to W, but yet Re and Os are attracted to SIA clusters while Ta is repelled. On the other hand, the binding property may also be related to the difference in atomic volume, with Re and Os being undersized and Ta being oversized compared to W. The correlation between solute-SIA binding characteristic with atomic volume, and lack of correlation with electronegativity, has been observed for various transition metals in W [24] as well as in Fe [37].

In Equation (4), the solute binding energy of a cluster in α configuration is calculated with respect to the corresponding α configuration of the pure cluster. This is necessary because solute replacement may induce translation of the dumbbells in the cluster along <111>. In this regard, we have carefully taken the following precaution. Whenever a translation occurs such that α configuration becomes β configuration, we replace the solute in the β configuration with W and

relax the configuration, if after the relaxation the pure cluster stays in β configuration, we take this β configuration as the reference in calculating the binding energy, if it relaxes back to α configuration, we take α configuration as the reference state. In addition, in a few replacement cases with Ta, the cluster instantaneously translates away from Ta. When this happens, the binding energy approaches zero. Therefore, we exclude such cases from the data collected in Table 4.

In the following paragraphs, we describe all instances of translation for the MSCs. For this purpose, the replacement sites are numbered (in black text) as shown in Figures 2, 3, and 5. In general, small clusters are more susceptible to translation, and Os and Ta are more likely to induce translation than Re. Furthermore, the most energetically favorable binding location for Re is usually the same for Os, which typically is the most energetically unfavorable site for Ta.

For MSC-2 (Figure 2b), the unique replacement sites are 1=4 and 2=3 (the = sign denotes equivalence). Rhenium and Ta at any of these sites do not cause translation. Osmium at site 2 causes itself to leave atom 1 to form a new mixed dumbbell with atom 1' and causes the 3-4 dumbbell to translate one hop along [111], such that the final configuration is equivalent to that if Os were placed at site 1. Site 1 provides the most binding for Re and Os and most repulsion for Ta.

For MSC-3 (Figure 3a), the unique replacement sites are 1=4, 2=3, and 5=6. Rhenium at any of these sites does not cause translation. Osmium at site 2 does not cause translation. Osmium at site 1 causes itself to form a new mixed dumbbell with its neighboring atom along [-1-11] and causes the 3-4 and 5-6 dumbbells to translate one hop along [-1-11] to form a final configuration that is equivalent to that of Os replacement at site 2. Osmium at site 5 causes translation to create an eventual configuration equivalent to Os replacement at site 2. Tantalum at any of the sites does not cause translation, except at site 1. At site 1, the cluster simply translates away, as a whole, from Ta. The strongest binding site for Re and Os is site 2. The strongest repulsion site for Ta is site 5.

For MSC-4 (Figure 5a), the unique replacement sites are 1=3, 2=4, 5, 6, 7, and 8. Rhenium and Os at any of these sites do not cause translation, except at site 5. At site 5, they cause 1-2 and 3-4 dumbbells to translate one hop along [11-1] to form a final configuration that is equivalent to replacement at site 7. Tantalum at sites 2, 6, and 8 does not cause translation. Tantalum at sites 1, 5, and 7 cause the whole cluster to translate away from the Ta. The strongest binding site for Re and Os is site 7. The strongest repulsion for Ta is at site 6. The weakest binding site for Re and Os, and weakest repulsion for Ta, is site 2.

For MSC-5 (Figure 4d), all replacement sites are unique. Rhenium at any site does not induce translation. Osmium does not cause any translation except at site 7. Osmium at site 7 causes all other dumbbells to translate one hop along [-1-11] to form an equivalent configuration to Os replacement at site 8. Tantalum also does not cause any translation except at site 7. Tantalum at site 7 causes atom 8 to leave the Ta and form a new dumbbell with its closest neighbor along [11-1]. The strongest binding for Re and Os, and the strongest repulsion for Ta, is at site 1. The weakest binding for Re and Os is at site 7. The weakest repulsion for Ta is site 8.

For MSC-6 (Figure 4g), the unique replacement sites are 1=2, 3=6, 4=5, 7=9, 8=10, 11, and 12. Rhenium and Os do not induce translation at any of these sites. Tantalum causes translation only at site 1 in which atom 2 leaves the Ta and forms a new dumbbell with its closest neighbor along [11-1]. The strongest binding for Re and Os, and the strongest repulsion for Ta, is at site 2. The weakest binding for Re and Os, and the weakest repulsion for Ta, is at site 11.

For MSC-7 (Figure 4j), the unique replacement sites are 1=3=5, 2=4=6, 7=10=14, 8=9=13, 11, and 12. Rhenium does not induce translation at any site. Osmium at site 1, 7, or 12 causes translation. At 1, it causes dumbbells 7-8, 9-10, and 11-12 to translate one hop along [-1-11]. At 7, it causes itself to leave atom 8 and to form a new mixed dumbbell with its nearest neighbor along [11-1], and causes all other dumbbells, except dumbbell 11-12, to translate one hop along [11-1], forming a final cluster equivalent to Os replacement at site 2. At site 12, Os causes dumbbells 1-2, 3-4, and 5-6 to translate one hop along [11-1]. Tantalum causes translation only at site 1 or 8, in which the cluster, as a whole, separates from the Ta. The strongest binding for Re and Os, and the strongest repulsion for Ta, is at site 2. The weakest binding for Re and Os, and the weakest repulsion for Ta, is at site 12.

It is interesting to relate the dumbbell sliding induced by a solute in several cases, as described above, to the transformation of the core configuration of a screw dislocation in bcc metals due to an interstitial solute (C, B, N, and O in Fe, and C in W) [38]. The solute causes the transformation from an easy-core configuration to a hard-core configuration. The two core configurations differ in the way the three nearest columns of atoms along <111> around the core are positioned along the <111> direction. It appears that the transformation is mediated by the sliding of these <111> columns, similar to the sliding of <111> dumbbells in our analysis above.

4. Discussion

We have explored cluster configurations up to size seven in which the binding energy of a size-n cluster with respect to the $n \rightarrow (n\text{-}1) + 1$ reaction is calculated through Equation (1). Figure 6 shows the average binding energy as a function of n, calculated from the three most stable clusters (Table 2), corresponding to the data with semicore states. In Figure 6, tic marks above and below the average values represent the maximum and the minimum values. Since the data are collected from the three most stable clusters, the maximum and minimum values correspond to the data from the first and the third most stable clusters, respectively. For $n > 7$, the binding energy may be calculated using the capillary approximation [23], in which the formation energy is proportional $n^{2/3}$. However this approximation may not be suitable for interstitial clusters studied here since these SIA clusters represent small nano-scale dislocation loops [34, 39], rather than spherical objects. The formation energy of a dislocation loop can be written as [40, 41]

$$E_f\{n\} = a\sqrt{n} + b\sqrt{n}\ln(n) \tag{5}$$

where a is the coefficient associated with the core-energy term and b is the coefficient associated with the elastic deformation energy of the medium surrounding the dislocation loop. The binding energy in Equation (1) can be rewritten as

$$E_b\{n\} = E_f\{1\} + E_f\{n-1\} - E_f\{n\} \tag{6}$$

Using Equation (5), Equation (6) becomes

$$E_b\{n\} = E_f\{1\} - a\left(\sqrt{n} - \sqrt{n-1}\right) - b\left(\sqrt{n}\ln(n) - \sqrt{n-1}\ln(n-1)\right) \tag{7}$$

The coefficients a and b may be fitted to the average binding energy data, or may be solved by using two values from those data. Since we are concerned with $n > 7$, we solve a and b using the data from the two largest clusters in this study, i.e. size-7 and size-6 clusters. The results are

$$a = \frac{E_f\{1\} - E_b\{7\} - 0.7595\ b}{0.1963} \tag{8}$$

$$b = \frac{0.2134(E_f\{1\} - E_b\{7\}) - 0.1963(E_f\{1\} - E_b\{6\})}{0.0070} \tag{9}$$

where, for the data with semicore states, $E_f\{1\}$ = 10.21 eV, $E_b\{7\}$ = 5.48 eV, and $E_b\{6\}$ = 4.96 eV yield a = 35.96 eV and b = -3.06 eV. With this model, the binding energy curve for $n > 7$ is plotted in Figure 6. For infinitely large clusters, the binding energy approaches the formation energy of a single <111> dumbbell [42].

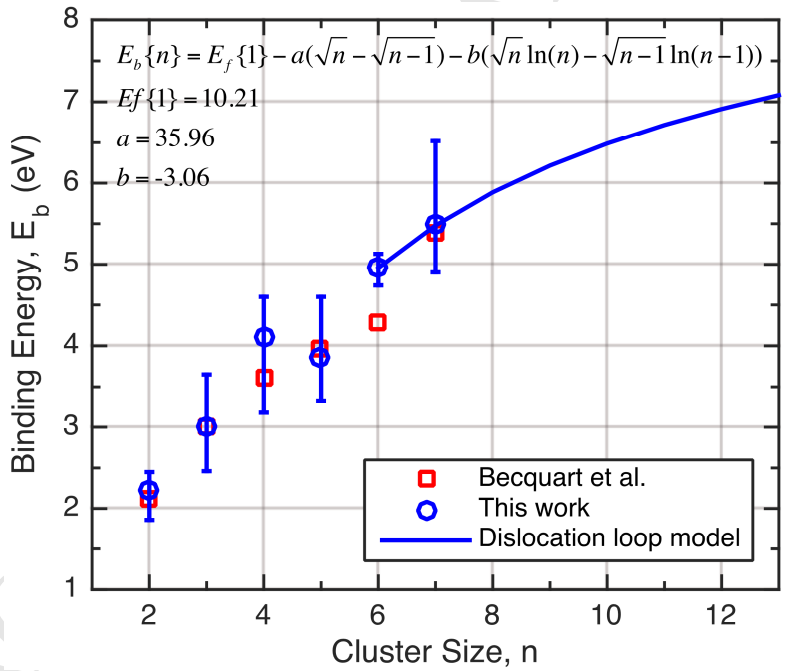

Figure 6. Binding energy of size-n SIA clusters with respect to an $n \rightarrow (n\text{-}1) + 1$ reaction. For this work, the data are extrapolated to an infinite supercell based on a finite size scaling and the calculations are performed with the 5p semicore states treated as valence states. For each cluster size, the average value over the three most stable clusters is plotted with the tic marks above and below the average values representing the maximum and the minimum values. For $n > 7$, an empirical formula as shown in the figure can be used. The formula is based on the formation energy of dislocation loops (see text). The formula is fit to the binding energy of size-6 and size-7 clusters, resulting in a = 35.96 eV and b = -3.06 eV. The asymptotic value is equal to the

formation energy of a single interstitial ([111] dumbbell) of $E_f\{1\}$ = 10.21 eV. For comparison, data points from [23] are plotted as squares.

In Figure 6, we compare the data from this study to those reported in [23] (squares). We find that the results from [23] generally fall within the range of the present results, except for n = 6 which is lower than our minimum value. Nevertheless, because the details of the configurations were not reported in [23] and that the calculations were performed with a different setup, without finite size scaling, and without semicore states, further assessment cannot be made.

So far, cluster stability is analyzed in terms of dissociation of one dumbbell from the cluster. Other processes can lead to different dissociation products. For instance, dissociation of a size-2, or a size-3 cluster from the parent cluster, and so on. It follows from Equation (6) that the larger the size of the dissociation product, the more energy needed. Therefore, the most likely dissociation mechanism is through a sequential process, involving one dumbbell at a time, even so, it is very unlikely given the strong binding of a single dumbbell.

The trend of the solute binding energy as a function of cluster size is depicted in Figure 7. As before, the data points are averaged from the results using the three most stable clusters (Table 4) and over different positions of the solute in the cluster. The maximum and minimum values show the range of the binding. From Figure 7, it is evident that as the cluster size increases, the binding decreases (for Re and Os). In addition, the variation of the binding at different replacement positions generally increases for larger clusters. A similar trend, but opposite sign, is obtained for Ta, i.e. the repulsion weakens for larger clusters.

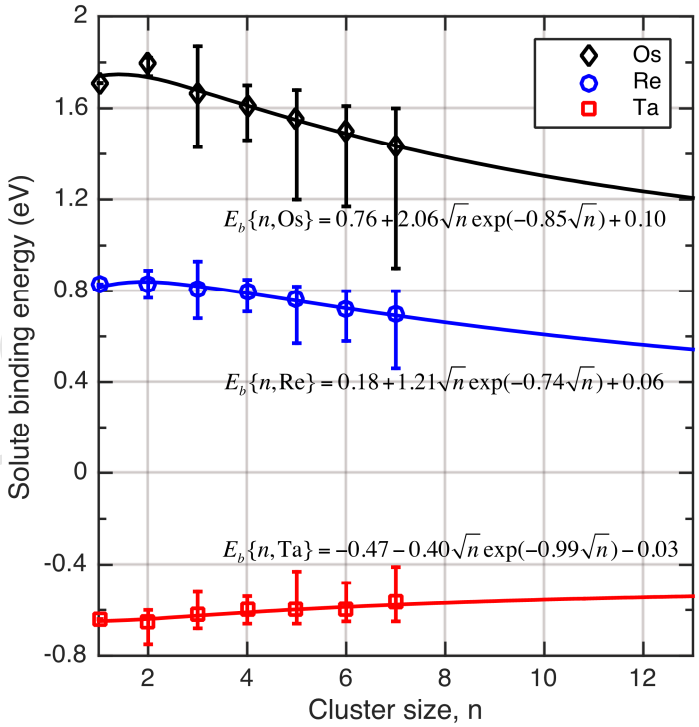

Figure 7. Binding energy of size-*n* SIA clusters to a Re, Os, or Ta atom substitutionally

replacing one of the W dumbbell atoms. The data points represent the average over the three most stable clusters. The tic marks represent the maximum and minimum values. The fit curves show the results of fitting the solute binding energy with an empirical formula of $E_b\{n, sol\} = E_{f,s} + c\sqrt{n}e^{-\beta\sqrt{n}} + d$, where $E_{f,s}$ is the formation energy of the substitutional solute and c, β, and d are the fitting parameters. The value of $E_{f,s}$, c, β, and d is, respectively, 0.18, 1.21, 0.74, 0.06 (for Re), 0.76, 2.06, 0.85, 0.10 (for Os), and -0.47, -0.40, 0.99, -0.03 (for Ta). The data are obtained from the calculations with finite-size correction and 5p semicore states.

From the data for size-7 clusters, it is found that the strongest binding is at the periphery of the cluster (seen from the projected view along the orientation of the dumbbells), or equivalently, the weakest binding occurs when the solute is in the middle of the cluster. In other words, the binding is strongest in regions with the largest stress field. The solute binding energy defined in Equation (4) can be rewritten in terms of formation energies, instead of total energies, as

$$E_b\{\alpha: n, sol\} = E_{f,s} + E_f\{\alpha: n\} - E_f\{\alpha: n, sol\} \tag{10}$$

The meaning of the notation is the same as in Equation (4). Deriving a physical model to describe the effect of a solute to the cluster's energetic proves to be very complex. As a first approximation, we express the difference in the formation energy between a pure cluster and a cluster with a solute for a size-n cluster as:

$$E_f\{\alpha: n\} - E_f\{\alpha: n, sol\} = c'\pi R^2 \frac{e^{-\beta' R}}{R} + d' = c\sqrt{n}e^{-\beta\sqrt{n}} + d \tag{11}$$

In the above equation, R denotes the radius of the cluster (assumed to be a circular loop). The first term is a product between the area of the cluster and the change in the formation energy per area caused by the charge density of the solute in which the influence of the solute is assumed to decay as a screened Coulomb interaction, i.e. $\sim \frac{\exp(-\beta' R)}{R}$. The second term, d, denotes the value of the formation energy change for an infinitely large cluster. The value of d is assumed to be constant because in an infinitely large cluster, every position of the solute in the cluster is equivalent. Furthermore, the value of d is non-zero because the strain field from an infinite array of [111] dumbbells is different from the strain field inside a bcc lattice, i.e. the formation energy of a solute within an infinite array of [111] dumbbells is different from the formation energy of a substitutional solute in a bcc lattice. Using this model, we fit the coefficients c, β, and d using the solute binding energy data as plotted in Figure 7. Table 6 summarizes the fit results along with the R^2 of the fit. We realize that this model lacks rigorous physical justifications. Surprisingly, however, the fit curves show that the model can well describe the trend of the solute binding energies.

Table 6. Fit results of the average binding energy, over the three most stable clusters, of size-n SIAs to a substitutional solute, using an empirical model of $E_b\{n, sol\} = E_{f,s} + c\sqrt{n}e^{-\beta\sqrt{n}} + d$, where $E_{f,s}$ is the formation energy of the substitutional solute and c, β, and d are the fitting parameters. Data are obtained from calculations with finite-size corrections and with 5p semicore states.

	Re	Os	Ta
$E_{f,s}$ (eV)	0.18	0.76	-0.47
c (eV)	1.21	2.06	-0.40
β	0.74	0.85	0.99
d (eV)	0.06	0.10	-0.03
R^2 of the fit	0.97	0.94	0.86

In this work, we include the results for which the solute is binding along the migration path of the clusters. Studying the binding properties for solute located perpendicular to the migration path of the clusters requires exploration of even larger sets of solute positions. For this reason, such study will be reserved for future work. Meanwhile, for a special case of an SIA dumbbell, the solute binding properties along parallel (//) as well as perpendicular (⊥) to the <111> direction have been reported [24]. It was found that at the first nearest site (⊥1), the binding for Ta, Re and Os is on the order of 0.2, 0.5 and 1.0 eV, respectively. However, the binding decreases rapidly towards zero for the second (⊥2) and third (⊥3) nearest site, suggesting that the interaction distance is very local, ~ 3 Å. On the other hand, the interaction distance along the // direction is much larger, ~ 15 Å. Given that the interaction range along a ⊥ direction is very local, one would expect that the behavior for larger clusters would be similar to that of a dumbbell. Note that while Ta strongly repels SIA clusters along the // direction, it was found to be attractive (E_b = ~0.2 eV) at ⊥1.

Consider an $\{\alpha{:}n,sol\}$ cluster, that is a size-n SIA cluster with one of the conjugate atoms replaced with a solute. We may ask the question what is the most energetically favorable dissociation product? Is it a substitutional solute, an SIA, or a mixed dumbbell? For simplicity, let's denote the binding energy associated with these three cases as $E_b\{n,sol\}$, $\mu_{db}\{n\}$, and $\mu_{dbx}\{n\}$, respectively, again the α configuration index has been omitted to indicate that these energies are average values over different configurations for each n. $E_b\{n,sol\}$ is the solute binding energy of an SIA cluster as defined in Equation (4). $\mu_{db}\{n\}$ and $\mu_{dbx}\{n\}$ are related to $E_b\{n,sol\}$ as

$$\mu_{dbx}\{n\} = E_b\{n,sol\} + E_b\{n\} - E_b\{1,sol\} \quad (12)$$

$$\mu_{db}\{n\} = E_b\{n,sol\} + E_b\{n\} - E_b\{n-1,sol\} \quad (13)$$

Where $E_b\{n\}$ is the binding energy of a size-n SIA cluster as defined in Equation (1). Note that $E_b\{1,sol\}$, which is the solute binding energy for a size-1 SIA cluster, is the same as the binding energy of a mixed dumbbell. Note that $E_b\{n,sol\}$ for Re, Os, and Ta have been plotted in Figure 7. Furthermore, the magnitude of $E_b\{n,sol\}$ is very small compared to μ_{db} and μ_{dbx}. Therefore, in Figure 8, only μ_{db} and μ_{dbx} are plotted. For Re and Os, $\mu_{db}\{n\} > \mu_{dbx}\{n\} >> E_b\{n,sol\}$, i.e. the most energetically favorable dissociation process is for the SIA cluster to separate, as a whole, from the solute. This conclusion is apparently valid also for Ta, since the cluster is repulsive to Ta. In a recent work [43], the binding properties of a pair of W-Re dumbbells were reported. The binding is analyzed with respect to separation into two individual W-Re dumbbells and can reach as high as 3.20 eV. Based on our comparison study of $E_b\{n,sol\}$, μ_{db} and μ_{dbx} above, the most energetically favored separation is when the whole SIA cluster detaches from the solute, leaving a substitutional Re. Therefore, it seems important to verify whether a cluster of two W-Re dumbbells would likely to separate into two individual W-Re dumbbells as analyzed in [43], or

to separate into a size-2 SIA cluster leaving behind two substitutional Re atoms. Indeed, future investigations are needed to elucidate the rich binding phenomena in complex W-Re clusters.

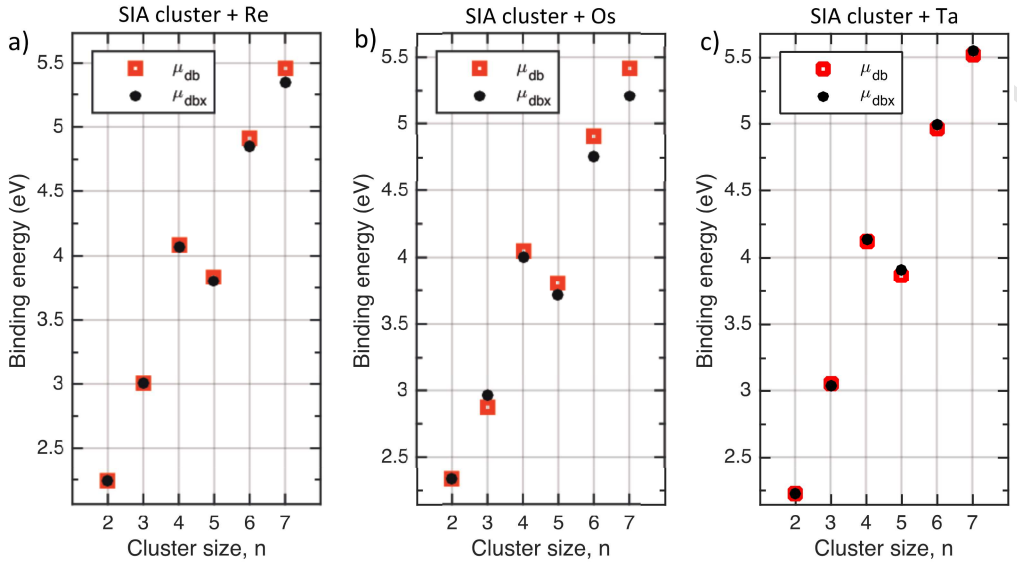

Figure 8. Binding energy of an {*n*,sol} cluster, i.e. a size-*n* SIA cluster with one solute replacing one of the dumbbells, with respect to two sets of products: a W-W dumbbell + {*n*-1,sol} with binding energy denoted as μ_{db} (plotted as red squares), or a W-sol mixed dumbbell + a size-(*n*-1) SIA cluster with binding energy denoted as μ_{dbx} (plotted as black dots). The solutes are Re, Os, or Ta. Data represent averages over three most stable clusters in each size and over different solute position within the cluster. The data are obtained from the calculations with finite-size correction and 5p semicore states.

Note that a mixed dumbbell migrates through a series of rotations between <111> and <110> with a barrier equal to the difference in the formation energy between the two orientations: 0.37, 0.07, and 0.34 eV for Ta, Re, and Os, respectively. On the other hand, an SIA can migrate through a rotation between <111> and <110> (with a barrier of 0.25 eV) and/or a translation along <111>. A calculation using the climbing nudged elastic band (cNEB) method gives the <111> migration barrier of 0.004 eV, compared to other plane-wave DFT results of 0.002 eV [30], 0.004 eV [44], and 0.005 eV [45]. The error of calculation in our simulation is on the order of 0.01 eV. Thus, the <111> migration barrier is negligible. A different ab initio study using a linear combination of atomic orbitals (LCAO) basis gives 0.05 eV [32] with the error in that calculation on the order of 0.015 eV. An experimental measurement suggests a value of 0.054 eV [25], but a more recent experiment shows that SIA migration is active even below 1.5 K [46] indicating that the barrier is close to zero. For SIA clusters, diffusion simulations with a classical interatomic potential shows that the diffusivity varies linearly with temperature [22], similar to the diffusion of an SIA [21]. In [21], the diffusivity data was fitted with a migration barrier of 0.013 eV and a pre-factor that varies linearly with temperature. From the above data, it is evident that the migration barrier of an SIA and SIA clusters is much smaller than that of a mixed dumbbell (i.e. the rotation barrier). Therefore, taking into account the migration barriers, in addition to the binding energies, the most energetically favorable dissociation path remains for the SIA cluster to separate, as a whole, from the solute.

5. Conclusions

We have explored a large number of candidate configurations of SIA clusters. The results show that small interstitial clusters prefer parallel <111> dumbbell orientations arranged in compact configurations on two or more {110} planes. These clusters are strongly binding. Three of the most stable clusters in each size of cluster have been used to obtain an average binding property. The binding energy of a size-n cluster with respect to $n \rightarrow (n\text{-}1) + 1$ reaction increases with size from approximately 2.24 eV (n = 2) to 5.48 eV (n = 7). For $n > 7$, an empirical model based on the formation energy of dislocation loops is presented as $E_b\{n\} = E_f\{1\} - a\left(\sqrt{n} - \sqrt{n-1}\right) - b(\sqrt{n}\ln(n) - \sqrt{n-1}\ln(n-1))$ where $E_f\{1\}$ = 10.21 eV is the formation energy of a [111] dumbbell and fitted parameters a = 35.96 eV and b = -3.06 eV. The model implies that the binding energy of an infinitely large cluster is equal to the formation energy of a [111] dumbbell.

The interaction of these clusters with Re, Os, or Ta substitutional solutes is studied by replacing one of the dumbbell atoms with the solute. It is found that these clusters are strongly attracted to Re and Os, but strongly repelled by Ta. The strongest interaction is found when the solute is located on the periphery of the cluster rather than in the middle of the cluster. Averaging over different positions of the solute in the cluster for the three most stable clusters in each cluster size shows that the solute binding energy decreases with cluster size from 0.83 eV (n = 1) to 0.70 eV (n = 7) for Re, from 1.71 to 1.43 eV for Os, and increases from -0.64 to -0.56 eV for Ta. The trend of the solute binding energy is well reproduced with a formula of $E_b\{n, sol\} = E_{f,s} + c\sqrt{n}e^{-\beta\sqrt{n}} + d$, where $E_{f,s}$ is the formation energy of the substitutional solute and c, β, and d are the fitting parameters. The value of $E_{f,s}$, c, β, and d is, respectively, 0.18, 1.21, 0.74, 0.06 (for Re), 0.76, 2.06, 0.85, 0.10 (for Os), and -0.47, -0.40, 0.99, -0.03 (for Ta). All the data are obtained from calculations with finite-size corrections and 5p semicore states included as valence states.

Acknowledgments

This research has been supported by the U. S. Department of Energy Office of Fusion Energy Sciences (#DE-AC06-76RL0-1830). Computations were performed on Olympus and Constance supercomputers at Pacific Northwest National Laboratory. The authors would like to acknowledge the use of OVITO [47] and SCIDAVIS [48] softwares for visualization and plotting.

References

[1] D. Stork, P. Agostini, J. L. Boutard, D. Buckthorpe, E. Diegele, et al., *Developing structural, high-heat flux and plasma facing materials for a near-term DEMO fusion power plant: The EU assessment*, Journal of Nuclear Materials **455**, 277 (2014).

[2] M. Rieth, S. L. Dudarev, S. M. Gonzalez De Vicente, J. Aktaa, T. Ahlgren, et al., *Recent progress in research on tungsten materials for nuclear fusion applications in Europe*, Journal of Nuclear Materials **432**, 482 (2013).

[3] A. R. Raffray, R. Nygren, D. G. Whyte, S. Abdel-Khalik, R. Doerner, et al., *High heat flux components—Readiness to proceed from near term fusion systems to power plants*, Fusion Engineering and Design **85**, 93 (2010).

[4] P. Norajitra, S. I. Abdel-Khalik, L. M. Giancarli, T. Ihli, G. Janeschitz, et al., *Divertor conceptual designs for a fusion power plant*, Fusion Engineering and Design **83**, 893 (2008).

[5] G. A. Cottrell, R. Pampin and N. P. Taylor, *Transmutation and Phase Stability of Tungsten Armor in Fusion Power Plants*, Fusion Science and Technology **50**, 89 (2005).

[6] M. R. Gilbert and J.-C. Sublet, *Neutron-induced transmutation effects in W and W-alloys in a fusion environment*, Nuclear Fusion **51**, 043005 (2011).

[7] A. Hasegawa, M. Fukuda, K. Yabuuchi and S. Nogami, *Neutron irradiation effects on the microstructural development of tungsten and tungsten alloys*, Journal of Nuclear Materials **471**, 175 (2016).

[8] A. Hasegawa, M. Fukuda, S. Nogami and K. Yabuuchi, *Neutron irradiation effects on tungsten materials*, Fusion Engineering and Design **89**, 1568 (2014).

[9] T. Tanno, A. Hasegawa, J.-C. He, M. Fujiwara, S. Nogami, et al., *Effects of Transmutation Elements on Neutron Irradiation Hardening of Tungsten*, Materials Transactions **49**, 2399 (2007).

[10] T. Tanno, A. Hasegawa, J. C. He, M. Fujiwara, M. Satou, et al., *Effects of transmutation elements on the microstructural evolution and electrical resistivity of neutron-irradiated tungsten*, Journal of Nuclear Materials **386**, 218 (2009).

[11] A. Hasegawa, M. Fukuda, T. Tanno and S. Nogami, *Neutron Irradiation Behavior of Tungsten*, Materials Transactions **54**, 466 (2013).

[12] T. Suzudo, M. Yamaguchi and A. Hasegawa, *Stability and mobility of rhenium and osmium in tungsten: first principles study*, Modelling and Simulation in Materials Science and Engineering **22**, 075006 (2014).

[13] L. R. Greenwood and F. A. Garner, *Transmutation of Mo, Re, W, Hf, and V in various irradiation test facilities and STARFIRE*, Journal of Nuclear Materials **212**, 635 (1994).

[14] W. Setyawan, A. P. Selby, N. Juslin, R. E. Stoller, B. D. Wirth, et al., *Cascade Morphology Transition in BCC Metals*, Journal of Physics: Condensed Matter **27**, 225402 (2015).

[15] W. Setyawan, G. Nandipati, K. J. Roche, H. L. Heinisch, B. D. Wirth, et al., *Displacement Cascades and Defects Annealing in Tungsten, Part I: Defect Database from Molecular Dynamics Simulations*, Journal of Nuclear Materials **462**, 329 (2015).

[16] G. Nandipati, W. Setyawan, H. L. Heinisch, K. J. Roche, R. J. Kurtz, et al., *Displacement Cascades and Defect Annealing in Tungsten, Part II: Object Kinetic Monte Carlo Simulation of Tungsten Cascade Aging*, Journal of Nuclear Materials **462**, 338 (2015).

[17] G. Nandipati, W. Setyawan, H. L. Heinisch, K. J. Roche, R. J. Kurtz, et al., *Displacement Cascades and Defect Annealing in Tungsten, Part III: the Sensitivity of Cascade Annealing*

in Tungsten to the Values of Kinetic Parameters, Journal of Nuclear Materials **462**, 345 (2015).
[18] R. W. Balluffi, *Vacancy defect mobilities and binding energies obtained from annealing studies*, Journal of Nuclear Materials **69**, 240 (1978).
[19] A. Satta, F. Willaime and S. De Gironcoli, *Vacancy self-diffusion parameters in tungsten: Finite electron-temperature LDA calculations*, Physical Review B **57**, 11184 (1998).
[20] C. S. Becquart and C. Domain, *Ab initio calculations about intrinsic point defects and He in W*, Nuclear Instruments and Methods in Physics Research Section B: Beam Interactions with Materials and Atoms **255**, 23 (2007).
[21] P. M. Derlet, D. Nguyen-Manh and S. L. Dudarev, *Multiscale modeling of crowdion and vacancy defects in body-centered-cubic transition metals*, Physical Review B **76**, 054107 (2007).
[22] S. L. Dudarev, *The non-Arrhenius migration of interstitial defects in bcc transition metals*, Comptes Rendus Physique **9**, 409 (2008).
[23] C. S. Becquart, C. Domain, U. Sarkar, A. Debacker and M. Hou, *Microstructural evolution of irradiated tungsten: Ab initio parameterisation of an OKMC model*, Journal of Nuclear Materials **403**, 75 (2010).
[24] X. S. Kong, X. B. Wu, Y. W. You, C. S. Liu, Q. F. Fang, et al., *First-principles calculations of transition metal-solute interactions with point defects in tungsten*, Acta Materialia **66**, 172 (2014).
[25] F. Dausinger and H. Schultz, *Long-Range Migration of Self-Interstitial Atoms in Tungsten*, Physical Review Letters **35**, 1773 (1975).
[26] G. Kresse and J. Furthmuller, *Efficient iterative schemes for ab initio total-energy calculations using a plane-wave basis set*, Physical Review B **54**, 11169 (1996).
[27] G. Kresse and D. Joubert, *From ultrasoft pseudopotentials to the projector augmented-wave method*, Physical Review B **59**, 1758 (1999).
[28] J. P. Perdew, K. Burke and M. Ernzerhof, *Generalized Gradient Approximation Made Simple*, Physical Review Letters **77**, 3865 (1996).
[29] H. J. Monkhorst and J. D. Pack, *Special points for Brillouin-zone integrations*, Physical Review B **13**, 5188 (1976).
[30] T. Ahlgren, K. Heinola, N. Juslin and A. Kuronen, *Bond-order potential for point and extended defect simulations in tungsten*, Journal of Applied Physics **107**, 033516 (2010).
[31] L. Gharaee and P. Erhart, *A first-principles investigation of interstitial defects in dilute tungsten alloys*, Journal of Nuclear Materials **467**, 448 (2015).
[32] D. Nguyen-Manh, A. P. Horsfield and S. L. Dudarev, *Self-interstitial atom defects in bcc transition metals: Group-specific trends*, Physical Review B **73**, 020101 (2006).
[33] L. Ventelon, F. Willaime, C.-C. Fu, M. Heran and I. Ginoux, *Ab initio investigation of radiation defects in tungsten: Structure of self-interstitials and specificity of di-vacancies compared to other bcc transition metals*, Journal of Nuclear Materials **425**, 16 (2012).
[34] S. L. Dudarev, *Coherent motion of interstitial defects in a crystalline material*, Philosophical Magazine **83**, 3577 (2003).
[35] P. H. Dederichs and J. Pollmann, *Elastic displacement field of point defects in anisotropic cubic crystals*, Zeitschrift für Physik **255**, 315 (1972).
[36] D. Grecu and P. H. Dederichs, *The asymptotic behaviour of the displacement field of point defects in 'isotropic' crystals*, Physics Letters A **36**, 135 (1971).

[37] P. Olsson, T. P. C. Klaver and C. Domain, *Ab initio study of solute transition-metal interactions with point defects in bcc Fe*, Physical Review B **81**, 054102 (2010).
[38] L. Ventelon, B. Lüthi, E. Clouet, L. Proville, B. Legrand, et al., *Dislocation core reconstruction induced by carbon segregation in bcc iron*, Physical Review B **91**, 220102 (2015).
[39] M. R. Gilbert, S. L. Dudarev, P. M. Derlet and D. G. Pettifor, *Structure and metastability of mesoscopic vacancy and interstitial loop defects in iron and tungsten*, Journal of Physics: Condensed Matter **20**, 345214 (2008).
[40] S. L. Dudarev, R. Bullough and P. M. Derlet, *Effect of the alpha-gamma Phase Transition on the Stability of Dislocation Loops in bcc Iron*, Physical Review Letters **100**, 135503 (2008).
[41] D. J. Bacon, R. Bullough and J. R. Willis, *Anisotropic Elastic Energy of a Rhombus-Shaped Dislocation Loop*, Philosophical Magazine **22**, 31 (1970).
[42] S. L. Dudarev, *Density Functional Theory Models for Radiation Damage*, Annual Review of Materials Research **43**, 35 (2013).
[43] L. Gharaee, J. Marian and P. Erhart, *The role of interstitial binding in radiation induced segregation in W-Re alloys*, Journal of Applied Physics **120**, 025901 (2016).
[44] X. S. Kong, Y. W. You, C. Song, Q. F. Fang, J. L. Chen, et al., *First principles study of foreign interstitial atom (carbon, nitrogen) interactions with intrinsic defects in tungsten*, Journal of Nuclear Materials **430**, 270 (2012).
[45] K. Heinola, T. Ahlgren, K. Nordlund and J. Keinonen, *Hydrogen interaction with point defects in tungsten*, Physical Review B **82**, 094102 (2010).
[46] H. Tanimoto, H. Mizubayashi, H. Nishimura and S. Okuda, *A Study of Self-Interstitial Atom in W by Means of Low-Temperature Irradiations*, Journal de Physique IV **6**, C8_285 (1996).
[47] A. Stukowski, *Visualization and analysis of atomistic simulation data with OVITO - the Open Visualization Tool*, Modelling and Simulation Materials Science and Engineering **18**, 015012 (2010).
[48] R. Standish, scidavis software, http://scidavis.sourceforge.net

- Systematic DFT exploration of tungsten SIA clusters from 1,264 configurations.
- Detailed structures of several most stable clusters are presented.
- Novel finding of the trend of solute binding of Re, Os, and Ta with SIA clusters.
- Empirical models that describe the trends of the solute binding energies.